

## Magnetic resonance imaging using linear magneto-inductive waveguides

R. R. A. Syms, I. R. Young, M. M. Ahmad, and M. Rea

Citation: *J. Appl. Phys.* **112**, 114911 (2012); doi: 10.1063/1.4768281

View online: <http://dx.doi.org/10.1063/1.4768281>

View Table of Contents: <http://jap.aip.org/resource/1/JAPIAU/v112/i11>

Published by the [American Institute of Physics](#).

---

### Related Articles

Automatic navigation of an untethered device in the artery of a living animal using a conventional clinical magnetic resonance imaging system

*Appl. Phys. Lett.* **90**, 114105 (2007)

Magnetic resonance-guided near-infrared tomography of the breast

*Rev. Sci. Instrum.* **75**, 5262 (2004)

Digital imaging processing for biophysical applications

*Rev. Sci. Instrum.* **75**, 2822 (2004)

Continuous wave optical spectroscopic system for use in magnetic resonance imaging scanners for the measurement of changes in hemoglobin oxygenation states in humans

*Rev. Sci. Instrum.* **74**, 4150 (2003)

$^3\text{He}$  spin exchange cells for magnetic resonance imaging

*J. Appl. Phys.* **92**, 1588 (2002)

---

### Additional information on *J. Appl. Phys.*

Journal Homepage: <http://jap.aip.org/>

Journal Information: [http://jap.aip.org/about/about\\_the\\_journal](http://jap.aip.org/about/about_the_journal)

Top downloads: [http://jap.aip.org/features/most\\_downloaded](http://jap.aip.org/features/most_downloaded)

Information for Authors: <http://jap.aip.org/authors>

## ADVERTISEMENT



**AIP Advances**

Now Indexed in  
Thomson Reuters  
Databases

Explore AIP's open access journal:

- Rapid publication
- Article-level metrics
- Post-publication rating and commenting

# Magnetic resonance imaging using linear magneto-inductive waveguides

R. R. A. Syms,<sup>1,a)</sup> I. R. Young,<sup>1</sup> M. M. Ahmad,<sup>1</sup> and M. Rea<sup>2</sup>

<sup>1</sup>*Optical and Semiconductor Devices Group, EEE Department, Imperial College London, Exhibition Road, London SW7 2AZ, United Kingdom*

<sup>2</sup>*Department of Radiology, Imperial College Healthcare NHS Trust, Praed St., Paddington, London W2 1NY, United Kingdom*

(Received 3 October 2012; accepted 1 November 2012; published online 11 December 2012)

Magneto-inductive waveguides are arrays of magnetically coupled, lumped element resonators, which support slow waves at radio frequency. Their use in internal magnetic resonance imaging (MRI), where they may provide an intrinsically safe method of signal detection and transmission, is described. A catheter-based receiver formed from a thin-film printed circuit mounted on a tubular scaffold using heat-shrink tubing is demonstrated, and its electrical response and imaging sensitivity are explained in terms of the excitation and propagation of magneto-inductive waves. The theoretical predictions are confirmed using the results of electrical measurement and <sup>1</sup>H MRI at 1.5 T, and imaging is achieved over a total length greater than 1.5 m using a single receiver.

© 2012 American Institute of Physics. [<http://dx.doi.org/10.1063/1.4768281>]

## I. INTRODUCTION

Following a suggestion by Pendry,<sup>1</sup> considerable attention has been paid to electrically resonant structures that provide controllable radio frequency (RF) permeability. Together with elements with controllable permittivity, these artificial media have led to the field of metamaterials. Early on, it was suggested that magnetic metamaterials might be used to duct RF flux during magnetic resonance imaging (MRI).<sup>2-4</sup> It was also suggested that images could be formed by point-to-point near field transfer,<sup>5-8</sup> rather than the conventional route of image recovery via Fourier transformation of encoded signals, and parallel imaging devices based on wire media have also been proposed.<sup>9-12</sup> A particular form of metamaterial, the magneto-inductive (MI) waveguide,<sup>13</sup> has also been used in a resonant ring detector<sup>14</sup> analogous to a bird-cage coil<sup>15,16</sup> but (by virtue of its lack of rigid connections) one that can be deformed to suit different imaging subjects.<sup>17</sup>

So far, these suggestions have had little impact. One reason is the bulky and unconventional nature of metamaterials. Another is their high loss, and correspondingly large noise factor.<sup>18,19</sup> For MRI, successful developments must be compatible with clinical procedures and lead to an increase in signal-to-noise ratio (SNR). There is, however, one area where metamaterials may have an advantage. It has long been known that small coils inserted directly into the body may increase SNR by virtue of their larger filling factor with the target tissue.<sup>20</sup> However, direct coupling of any inserted coil or cable to either the B<sub>1</sub> field or the E field of the powerful MRI transmitter can lead to rapid heating. Segmentation of cables using transformers,<sup>21</sup> especially with figure-of-eight winding,<sup>22</sup> has been proposed as a solution. A periodic structure of this type is clearly a metamaterial and represents an application where a small reduction in performance may be justified by a further consideration, patient safety. However,

because all demonstrated devices have been large, usable detectors based on this approach have yet to be demonstrated.

We have recently developed a compact catheter receiver for internal MRI that appears extremely promising for biliary or vascular imaging, based on a thin film magneto-inductive waveguide.<sup>23</sup> The design allows imaging and catheter visualisation over an extended length, with a field of view that consists of a narrow cylinder running coaxial to the catheter, even when the catheter track is bent. The waveguide provides protection against external fields, and inductive coupling at the output introduces additional patient safety. Initial work has focused on the clinical background, device construction, and demonstration of a MR imaging performance appropriate to the clinical task.<sup>24</sup> The aim of the present work is to explain the physics of signal detection, which involves the excitation and propagation of magneto-inductive waves. Section II briefly describes the device and develops an equivalent circuit model for signal detection to predict its response. Section III confirms the model predictions with the results of electrical characterisation and MR imaging experiments using phantoms. Sec. IV presents conclusions.

## II. MAGNETO-INDUCTIVE CATHETER RECEIVER

In this section, we present the device itself and a simple equivalent circuit that supports MI waves and use the model to simulate transmission between an electrical source and the load.

### A. Device design

The magneto-inductive catheter receiver consists of a thin film circuit wrapped round a tubular scaffold and held in place with heat shrink tubing, as shown in Figure 1(a). The circuit is based on earlier thin-film MI waveguides<sup>23</sup> and contains a linear array of L-C resonators formed partly on the front and partly on the back of a thin substrate as shown in Figure 1(b). Conductive loops provide inductors, and conductive strips separated by the dielectric substrate act as

<sup>a)</sup>Author to whom correspondence should be addressed. Electronic mail: r.syms@imperial.ac.uk. Tel.: +44-207-594-6203. Fax: +44-207-594-6308.

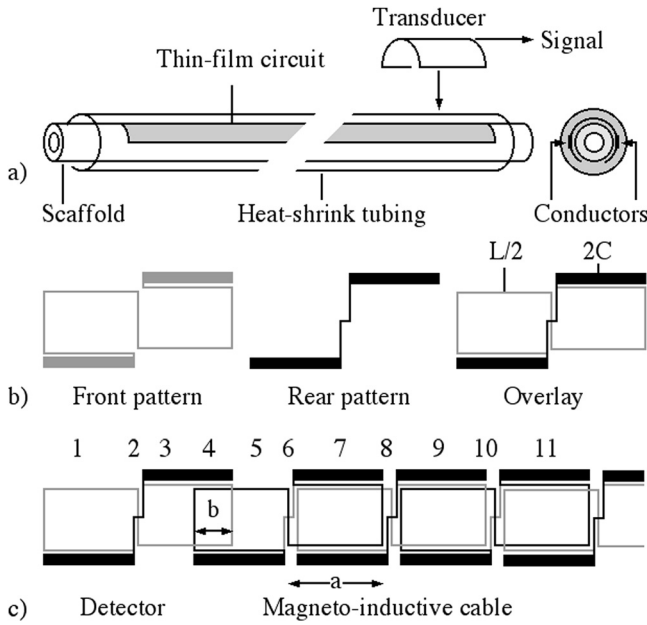


FIG. 1. (a) Construction of magneto-inductive catheter receiver, (b) conductor layout for a single resonator, and (c) layout of overall thin film circuit.

parallel-plate capacitors. Each loop is separated into two inductors of value  $L/2$  combining to a total of  $L$  and two capacitors of value  $2C$  combining to a total of  $C$ . This arrangement obviates the need for any vias or airbridges to complete the circuit and allows it to be fabricated simply using double-sided patterning of copper. The long conductors are placed on the diameter of the tubular scaffold, so that uniform sections act like single-turn rectangular loops, with a similar local transverse variation in sensitivity. However, the use of figure-of-eight shaped elements provides protection against uniform external  $B_1$  fields acting over an extended length during the excitation phase of MRI.

Each resonator is coupled to its neighbour by overlaying the two as shown in Figure 1(c) so that their magnetic fields interact, but using a lateral offset of one conductor width to reduce the effect of parasitic capacitance. Segmentation provides protection against external E-fields acting parallel to the long conductors, since the length over which common-mode standing waves may be excited is now short. The combined circuit is clearly capable of inductive detection and signal propagation along its length. However, the details of the magnetic couplings affect both aspects, leading to an axial variation in sensitivity that we now consider.

## B. Equivalent circuit

Figure 2(a) shows the equivalent circuit of the receiver. Within the cable, the mutual inductance between neighbours is  $M$ . The current  $I_n$  in the  $n$ th element at angular frequency  $\omega$  is then related to the currents  $I_{n-1}$  and  $I_{n+1}$  and any imposed voltage  $V_n$  by the recurrence equation

$$(j\omega L + j\omega C + R)I_n + j\omega M(I_{n-1} + I_{n+1}) = V_n. \quad (1)$$

With no imposed voltage, assumption of the traveling current wave solution  $I_n = I_0 \exp(-jnka)$ , where  $k$  is the propagation constant and  $a$  is the period, leads to the dispersion equation

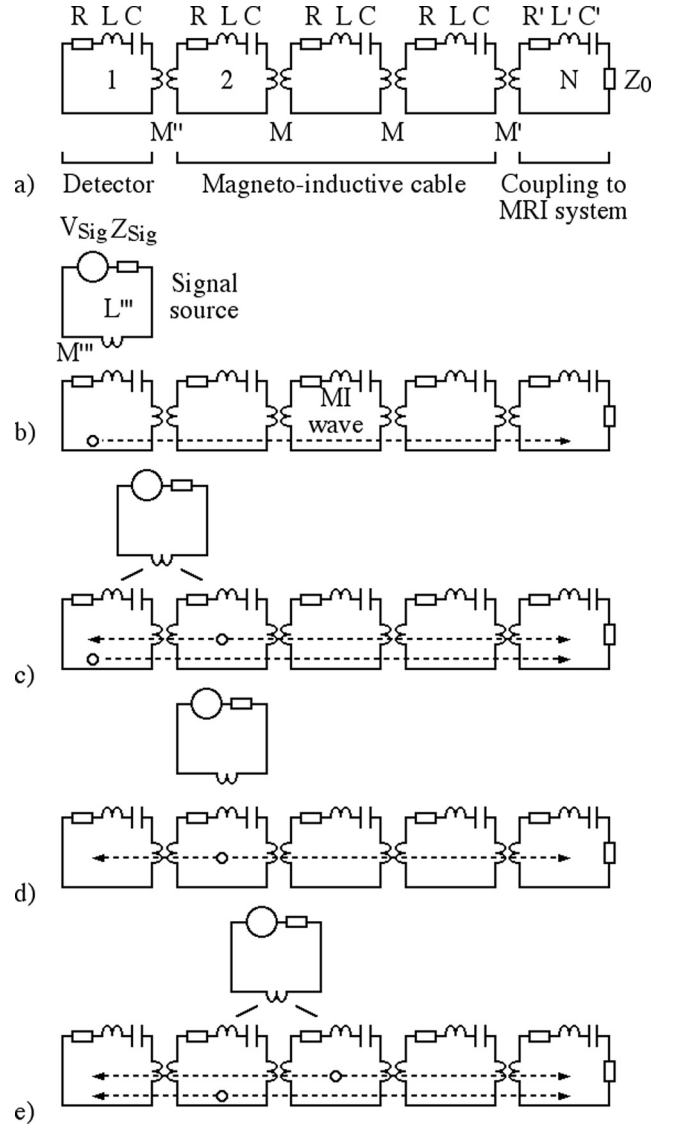


FIG. 2. Equivalent circuit of (a) receiver; (b)-(e) receiver with signal source near regions 1, 4, 5, and 7 of Figure 1(c).

$$(1 - \omega_0^2/\omega^2 - j/Q) + \kappa \cos(ka) = 0. \quad (2)$$

Here  $\omega_0 = 1/\sqrt{LC}$  is the angular resonant frequency of the loops,  $Q = Q_0\omega/\omega_0$ , where  $Q_0 = \omega_0 L/R$  is the quality factor, and  $\kappa = 2M/L$  is the coupling coefficient. Defining the complex propagation constant  $k = k' - jk''$  and assuming low loss then leads to the approximations

$$\begin{aligned} (1 - \omega_0^2/\omega^2) + \kappa \cos(k'a) &= 0 \\ k''a &= 1/\{kQ \sin(k'a)\}. \end{aligned} \quad (3)$$

The upper equation is the dispersion equation for lossless MI waves and implies that for positive  $\kappa$  (as here) propagation is only possible over the frequency range  $1/\sqrt{1+\kappa} \leq \omega/\omega_0 \leq 1/\sqrt{1-\kappa}$ . The lower equation gives the loss variation and implies that  $k''a$  is minimum at resonance when  $k'a = \pi/2$  and has the value  $1/\kappa Q_0$ . Low loss therefore requires a high quality factor and a large value of  $M$ . It is simple to show that the characteristic impedance of the

waveguide is  $Z_0 = j\omega M \exp(-jka)$ , which at resonance reduces to the real value  $Z_{0M} = \omega_0 M$ .

The first resonator acts as the main detector. For simplicity, exactly the same element is used. However, rather than being simply uniform, the waveguide is made self-terminating, and the detector is coupled to the cable by a different mutual inductance  $M''$ . Assuming that it acts as source with output resistance  $R$ , impedance matching between the detector and the cable is achieved at resonance if  $\omega_0 M'' = \sqrt{RZ_{0M}}$ . Since  $R$  is typically small,  $M''$  must be relatively weak. This condition can be easily satisfied, by making the dimension  $b$  in Figure 1(c) relatively small compared with the period  $a$ . For the detector and the first cable element, the circuit equations are

$$\begin{aligned} (j\omega L + 1/j\omega C + R)I_1 + j\omega M'' I_2 &= V_1, \\ (j\omega L + 1/j\omega C + R)I_2 + j\omega M'' I_1 + j\omega M I_3 &= V_2. \end{aligned} \quad (4)$$

The demountable transducer is a two-turn spiral inductor made resonant with thin film capacitors, and having equivalent circuit parameters  $R'$ ,  $L'$ , and  $C'$ . This element uses a mutual inductance  $M'$  to couple the cable to the scanner electronics, which have input impedance  $Z_0$ . Matching is obtained at resonance if  $\omega_0 M' = \sqrt{Z_0 Z_{0M}}$  and can be achieved by adjusting the transducer position. Assuming a total of  $N$  elements, the circuit equations for the last cable element and the transducer are

$$\begin{aligned} (j\omega L + 1/j\omega C + R)I_{N-1} + j\omega M I_{N-2} + j\omega M' I_N &= V_{N-1}, \\ (j\omega L' + 1/j\omega C' + R')I_N + j\omega M' I_{N-1} &= V_N. \end{aligned} \quad (5)$$

Typically, the voltages  $V_1 \dots V_{N-1}$  will be detected MR signals, while  $V_N$  will be zero. A MR signal source can be represented as a loop containing a RF voltage  $V_{\text{sig}}$  with impedance  $Z_{\text{sig}}$  and an inductance  $L'''$  as shown in Figures 2(b)–2(e), allowing the source to be coupled to elements in the detection circuit via a mutual inductance  $M'''$ . Clearly, a realistic source would be made resonant with a further capacitor  $C'''$ , but the arrangement here allows broadband excitation. At least approximately, the effect of the source is to couple into any nearby element a voltage  $V_S = j\omega_0 M''' V_{\text{sig}} / Z_{\text{sig}}$ , together with an associated resistance (the body loading in MRI) that we ignore for simplicity.

### C. Excitation of magneto-inductive waves

For a group of spins near any loop crossover (positions 2, 6, 8, and 10 in Figure 1(c)), equal and opposite voltages will be induced in the two halves of the loop concerned. We will ignore these cases, since the signals will cancel. For spins near the left-hand loop of the detector (position 1) the source is only coupled to the first resonator, as shown in Figure 2(b). All the imposed voltages will be zero, except  $V_1 = V_S$ . This voltage will excite a single MI wave, which will travel towards the load where it will be absorbed. For spins near position 3, the situation will be similar. For spins near the junction between the cable and detector (position 4), the source is coupled to both the first and second resonators,

as in Figure 2(c). Three waves will now be generated: a single wave from the first element, and a pair of counter-propagating waves from the second. For spins near positions 5 and 7, the situation is as shown in Figures 2(d) and 2(e). In each case, a number of MI waves will be excited, and the detected signal will be the sum of those that reach the load. Because the number varies, we would also expect the detection sensitivity to vary.

At resonance, the backward-going waves will be absorbed in the detector and therefore may be ignored. Off-resonance, the situation will be more complicated. Because the terminating elements are no longer impedance-matched, each wave may suffer multiple internal reflections. However, the response may always be found by writing Eqs. (1), (4), and (5) in the form  $\mathbf{Z}\mathbf{I} = \mathbf{V}$ , where  $\mathbf{Z}$  is a matrix containing impedances,  $\mathbf{I}$  is a column vector of unknown currents, and  $\mathbf{V}$  is a similar column vector of imposed voltages. Inversion yields the currents as  $\mathbf{I} = \mathbf{Z}^{-1}\mathbf{V}$ . Using the source model presented here, the system transmission (which is proportional to the detection sensitivity) may then be found. For comparison with experimental receivers, the following normalised parameter values may be assumed:  $f_0 = \omega_0/2\pi = 63.8$  MHz,  $Z_0 = 50 \Omega$ ,  $Z_{0M} = 40 \Omega$ ,  $\kappa = 0.6$ ,  $Q_0 = 40$  and 15 elements. For comparison with sensitivity measurements made with an electronic network analyser, the following additional parameters may be assumed for the signal source:  $Z_{\text{sig}} = 50 \Omega$ ,  $L''' = L/20$ , and  $M''' = 0.02\sqrt{LL''}$ .

### D. Simulated response

The full line in Figure 3 shows the simulated variation in transmission with source position. Here we have ignored the signal nulls and have assumed that  $b/a = 0.5$  for the purpose of presentation. These results show clearly that while the receiver can detect signals along its entire length, the sensitivity is not uniform. Transmission is highest when the source is near the detector (positions 1 and 3), because external signals in this region excite voltages from a source that is

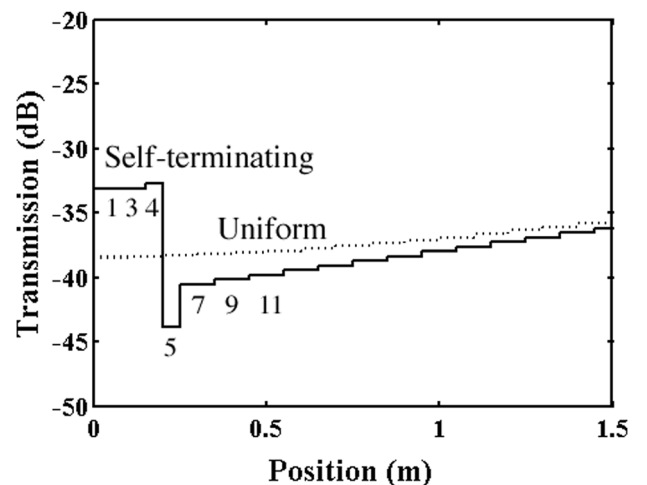


FIG. 3. Theoretical variation of system transmission with axial position of the source, at resonance. Full lines: self-terminating system; dotted lines: uniform system. The values at the nodes 2, 6, 8, 10... where the signal is cancelled have been omitted for clarity.

impedance matched to the load. There is a slight increase where the detector attaches to the cable (position 4), due to the generation of an additional MI wave in the first cable element. This wave is excited less efficiently, because the cable elements are not impedance-matched sources. However, due to the  $\pi/2$  phase delay between elements, it is in quadrature with the wave from the detector and their powers add. Transmission falls abruptly when the source is near the remainder of the first cable element (position 5), because only the weakly excited MI wave is generated. After that, transmission rises by around 3 dB in the second cable element, because two weak waves are now generated in quadrature. Transmission then climbs linearly in the remainder of the cable as propagation losses reduce.

In this configuration, the system is exactly analogous to the conventional one of a resonant detector that is impedance matched to a transmission line, which is then itself matched to a load. Clearly, other arrangements are possible. For example, the overlay *b* could be chosen so that the mutual inductance  $M''$  matches that of the rest of the line. The dotted line in Figure 3 shows the simulated variation in transmission, assuming that *b* has now altered appropriately to *a*. In this case, the advantages of tip resonance are clearly lost, and (apart from the effects of loss) the detection sensitivity is approximately uniform. Alternatively the entire line could be made resonant. Desirable as though this sounds, propagation losses of MI waves are sufficiently high as to render this arrangement impractical.

Figure 4 shows simulated variations in transmission with frequency, for different source positions. The variations change in a complicated manner. The bold line in Figure 4(a) shows results for the detector (position 1). Here, the response is clearly resonant, peaking at the design frequency. However, some transmission is obtained over the whole MI wave band. Oscillations at high frequency can be ascribed to multiple reflections, due to poor impedance matching off resonance. The remainder of Figures 4(a) and 4(b) show similar results obtained with the external source in positions 4, 5, 7, 9, and 11. In each case, the signal source is coupled to more than one element, as necessary. The responses are now entirely different. The dotted line in Figure 4(a) shows the response at position 4, where the detector is connected to the cable. There is still a semblance of resonance, but the overall response is much broader, with significant transmission over the whole MI band. There is a deep null just above the resonant frequency. In positions 5–11, the resonance has disappeared entirely. Instead, the response is generally broad and low, with nulls of varying depth at intervals across the pass-band. These effects can be ascribed to cancellation of the MI waves traveling towards the load by backward-going waves reflected from the detector, which is only matched at resonance.

### III. EXPERIMENTAL DEMONSTRATION

In this section we describe the experimental realisation of the receiver and compare the measured electrical response and the results of magnetic resonance imaging experiments with the predictions of Sec. II.

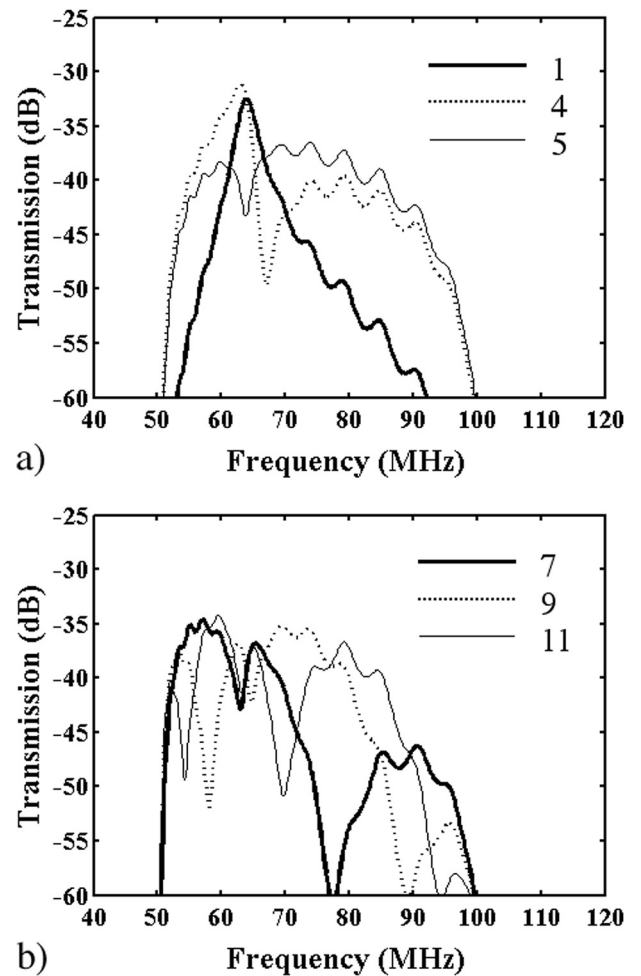


FIG. 4. Theoretical variation of system transmission with frequency, with the signal source at different axial locations in Figure 1(c): (a) positions 1, 4, and 5; (b) positions 7, 9, and 11.

#### A. Device construction

Magneto inductive catheter receivers were fabricated in arrays using double-sided patterning and etching of copper-clad Kapton with  $35\ \mu\text{m}$  Cu and  $25\ \mu\text{m}$  polyimide thickness. Layout parameters were chosen to achieve component values suitable for operation at 63.8 MHz frequency (as required for  $^1\text{H}$  MRI in a 1.5 T magnetic field). Inductor track widths were 0.5 mm, and capacitors were formed using strips of 0.75 mm width. The overall device length was over 1.6 m and was achieved using 15 elements with a width of 3.5 mm, an overall length of 200 mm, and a period of  $a = 100\ \text{mm}$ . The overall loop inductance was  $L \approx 0.3\ \mu\text{H}$ , and the loop resistance around  $3\ \Omega$ . The circuits were separated using a scalpel, the capacitors were mechanically trimmed slightly to set the resonant frequency, and each circuit was attached to a 2.25 mm diameter PTFE tube using heatshrink tubing.

Each thin film circuit consisted of a single, continuous double-sided print, with an overall width slightly less than one catheter circumference. The circuits were wrapped around the catheter so that the direction of MI wave propagation lay parallel to the axis of the catheter and the long conductors of the inductors lay on either side of a diameter as previously shown in Figure 1(a). The short perpendicular

conductors then formed half circles passing over the top of the catheter. Despite this, the flattened representation of Figure 1(c) remained a good approximation. Accurate co-axial alignment was achieved by mounting the catheter on a taught wire jig during the assembly process. For experimental purposes, it was helpful to avoid twists in the circuit; however, these did not alter electrical operation. In practice it was simple to ensure a linear arrangement using a transparent heat-shrink sleeve.

The inductive coupling transducer was constructed from a two-turn thin-film inductor of length 100 mm, which was also equipped with thin film capacitors for resonance. This circuit was epoxied onto the inside of a split Perspex clamp equipped with a SMA-type RF connector.

## B. Electrical evaluation

Electrical evaluation was carried out with an Agilent E5061A electronic network analyser (ENA), using a small inductive loop for excitation. Catheters were taped down onto the laboratory bench, and their response measured with the excitation source in the positions previously shown in Figure 1(c). Figure 5 shows the variation of the transmission from the ENA (acting as the signal source) to itself (acting as the load) with axial position of the loop. This figure should be compared with the full line in Figure 3. The main features of the theoretical response (high sensitivity at the tip, followed by a large drop at the cable connection element) are largely replicated. However, the peak sensitivity is somewhat lower, the rate of increase of signal along the cable is higher, and minor oscillations indicate a slight lack of impedance matching.

The transmission loss in the cable section appears to be at least 7 dB. For comparison, the loss of an equivalent, continuous length of sub-miniature coaxial cable (0.8 mm diameter, 50  $\Omega$  Bluetooth, Axon Cable Ltd., Dunfermline, UK) at 63.8 MHz was measured as  $\approx 1$  dB, illustrating the loss penalty associated with the metamaterial construction.

Figures 6(a) and 6(b) show experimental measurements of sensitivity with frequency, obtained at the same locations

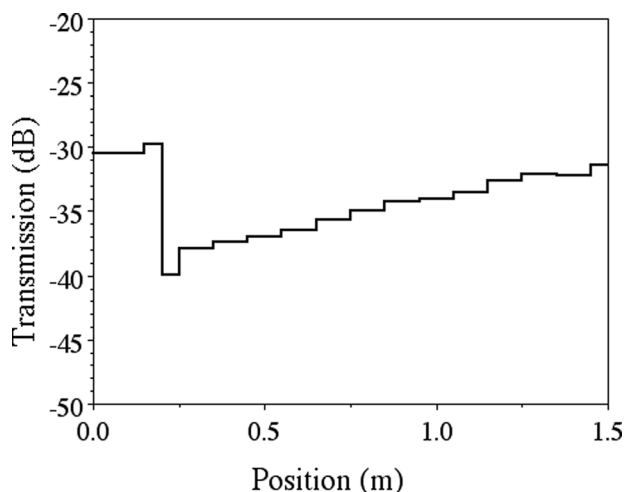


FIG. 5. Experimental variation of system transmission with axial position of the source, at resonance. The values at the nodes where the signal is cancelled again have been omitted for clarity.

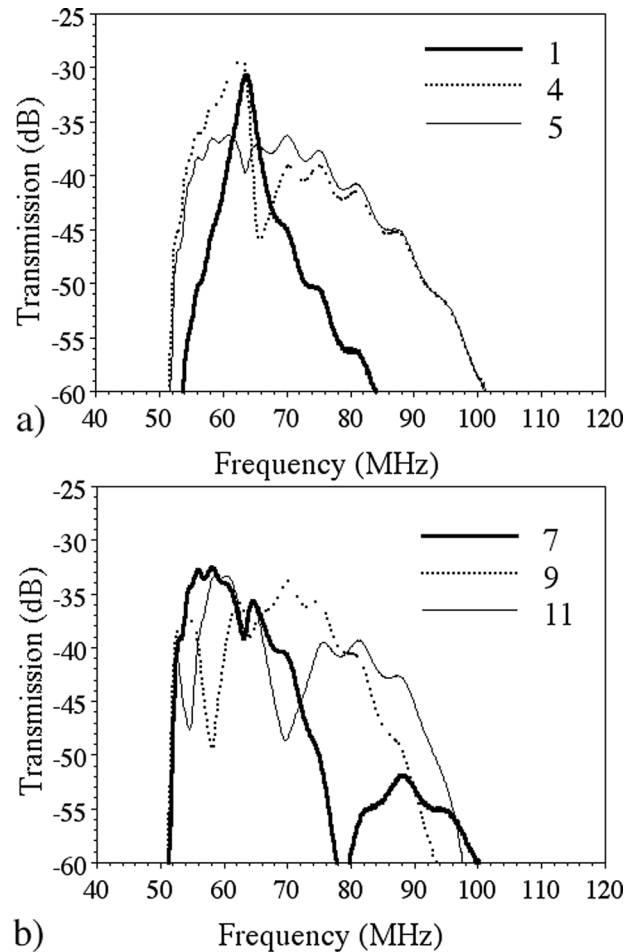


FIG. 6. Experimental variation of system transmission with frequency, with the signal source at different axial locations in Figure 1(c): (a) positions 1, 4, and 5; (b) positions 7, 9, and 11.

as Figures 4(a) and 4(b). The qualitative agreement is excellent. All the main features of the predicted response are again present, including the complicated distributions of signal nulls. The main discrepancy appears to be a reduction in the experimental transmission at high frequency. The most likely explanation is rising loss due to the skin effect, which is omitted from the model.

## C. Magnetic resonance imaging

$^1\text{H}$  magnetic resonance imaging was carried out at St. Mary's Hospital, Paddington, London, using a 1.5 T GE Signa Excite clinical scanner. The subject was a cuboid phantom, filled with a solution containing 3.37 g/l  $\text{NiCl}_2 \cdot 6\text{H}_2\text{O}$  and 2.4 g/L NaCl (with  $T_1 = 500\text{--}800$  ms and  $T_2 = 100\text{--}200$  ms). The catheter coil was taped on top of the phantom in a spiral racetrack arrangement as shown in Figure 7(a). The assembly was then positioned at the magnet isocentre. The system body coil was used for excitation, and the catheter receiver was connected to an auxiliary coil input for signal reception.

Imaging was carried out using a 2D spin echo sequence, with a repetition time  $\text{TR} = 520$  ms, an echo time  $\text{TE} \approx 8.088$  ms, an echo train length  $\text{ETL} = 2$ , 50% phase field of view, and  $90^\circ$  flip angle. Slices were acquired in the coronal plane, with a slice thickness of 5 mm and a slice

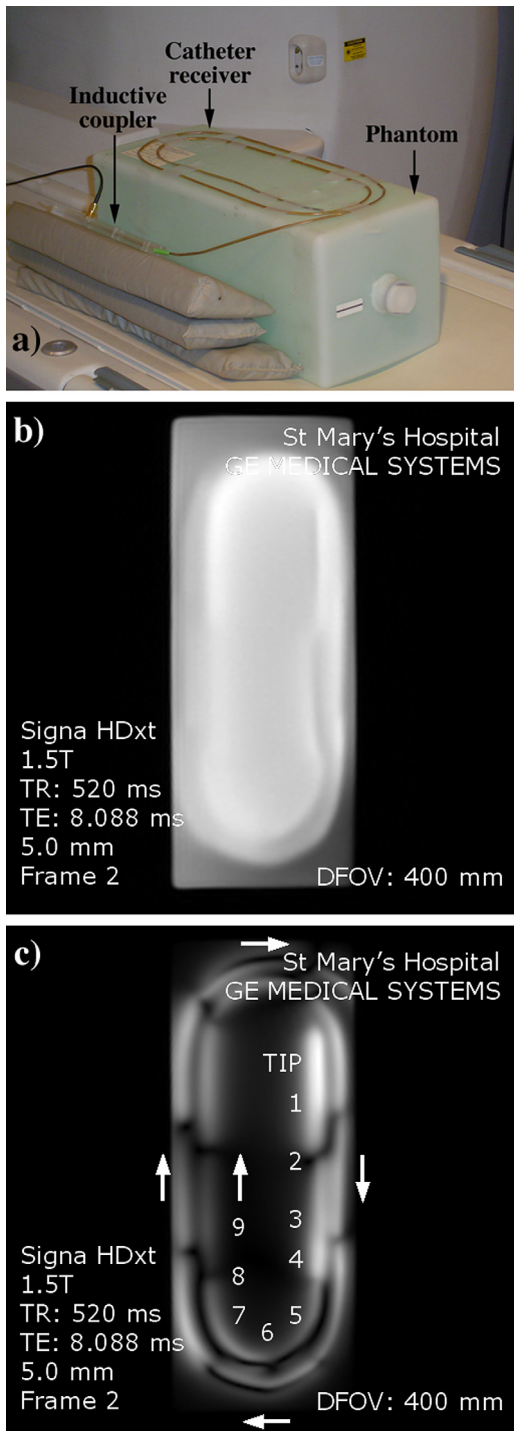


FIG. 7. (a) Arrangement for  $^1\text{H}$  magnetic resonance imaging at 1.5T; (b) and (c) coronal MR images obtained using the body coil and magneto-inductive catheter receiver, respectively.

separation of 5.2 mm. 8 excitations were used to improve signal-to-noise ratio.

Figure 7(b) shows a coronal slice image of the liquid below the catheter, obtained using the body coil. The limited degree of perturbation to the image brightness suggests that the decoupling expected from the figure-of-eight-shaped elements does operate reasonably well, but (by comparison with other experiments carried out with a straight catheter) is less effective with a curved arrangement.

Figure 7(c) shows the corresponding slice image obtained using the catheter coil. The image clearly consists of a track that follows the layout of the catheter. The track is multi-lobed, with each lobe corresponding to one half of a figure-of-eight element and the dark spaces between corresponding to the track crossover regions. A total of 15 separate lobes may be identified, implying imaging over a total distance of at least 1.5 m. The imaging locations identified in Figure 1 may be easily recognised and are marked, together with the direction of signal propagation.

The difficulty of exactly aligning the slice plane with the top of the phantom (which is itself not truly planar) make it hard to extract a detailed brightness variation for comparison with Figure 3(a). However, the image is clearly brightest in locations 1, 3, and 4. There is then an abrupt reduction in brightness in location 5, and a reasonably steady rise in brightness thereafter. On this basis, the experimentally measured variation in detection sensitivity maps at least qualitatively onto a variation in imaging sensitivity, even in an arrangement such as this, with extreme bending.

#### IV. CONCLUSIONS

We have demonstrated a novel catheter-based receiver for  $^1\text{H}$  internal magnetic resonance imaging at 1.5T, based on a self-terminating magneto-inductive waveguide. Segmentation of the circuit into resonant elements with a controllable layout (a figure-of-eight loop) is used to avoid direct coupling to external E and  $B_1$  fields and hence provide inherent patient protection. Consequently, this device may represent a useful application for RF metamaterial despite the increase in transmission loss over a comparable system based on a coaxial output cable. A simple equivalent circuit model for signal detection has been presented. The predicted performance is confirmed using the results of electrical measurement and MRI, and imaging is achieved over a total length greater than 1.5 m. Signal detection is by excitation of magneto-inductive waves. The number of waves and the efficiency with which they are excited varies from element to element along the waveguide, and these differences give rise to the experimentally observed variation in detection sensitivity.

#### ACKNOWLEDGMENTS

The Authors are extremely grateful to the Wellcome Trust for financial support, to Professor Wady Gedroyc for access to MR imaging facilities, and to Professor Laszlo Solymar, Dr. Ekaterina Shaminina, and Dr. Mike Wiltshire for valuable discussions.

<sup>1</sup>J. B. Pendry, A. J. Holden, D. J. Robbins, and W. J. Stewart, "Magnetism from conductors and enhanced nonlinear phenomena," *IEEE Trans. Microwave Theory Tech.* **47**, 2075–2084 (1999).

<sup>2</sup>M. C. K. Wiltshire, J. B. Pendry, I. R. Young, D. J. Larkman, D. J. Gilderdale, and J. V. Hajnal, "Microstructured magnetic materials for RF flux guides in magnetic resonance imaging," *Science* **291**, 849–851 (2001).

<sup>3</sup>M. C. K. Wiltshire, R. M. Henkelman, I. R. Young, and J. V. Hajnal, "Metamaterial yoke for signal reception—An initial investigation," in *Proceedings of ISMRM 11*, Toronto, Canada, 10–16 July, 2003, p. 43.

- <sup>4</sup>M. C. K. Wiltshire, E. Shamonina, I. R. Young, and L. Solymar, "Resonant magnetic concentrators," in PIERS Symposium, Honolulu, Hawaii, 13–16 October 2003.
- <sup>5</sup>M. C. K. Wiltshire, J. V. Hajnal, J. B. Pendry, D. J. Edwards, and C. J. Stevens, "Metamaterial endoscope for magnetic field transfer: Near field imaging with magnetic wires," *Opt. Express* **11**, 709–715 (2003).
- <sup>6</sup>F. Mesa, M. J. Freire, R. Marques, and J. D. Baena, "Three-dimensional superresolution in metamaterial slab lenses: Experiment and theory," *Phys. Rev. B* **72**, 235117 (2005).
- <sup>7</sup>M. J. Freire, R. Marques, and L. Jelinek, "Experimental demonstration of a  $\mu = -1$  metamaterial lens for magnetic resonance imaging," *Appl. Phys. Lett.* **93**, 231108 (2008).
- <sup>8</sup>M. J. Freire, L. Jelinek, R. Marques, and M. Lapine, "On the applications of  $\mu_r = -1$  metamaterial lenses for magnetic resonance imaging," *J. Magn. Reson.* **203**, 81–90 (2010).
- <sup>9</sup>P. A. Belov, Y. Hao, and S. Sudhakaran, "Subwavelength microwave imaging using an array of parallel conducting wires as a lens," *Phys. Rev. B* **73**, 033108 (2006).
- <sup>10</sup>P. A. Belov, Y. Zhao, S. Sudhakaran, A. Alomainy, and Y. Hao, "Experimental study of the subwavelength imaging by a wire medium slab," *Appl. Phys. Lett.* **89**, 262109 (2006).
- <sup>11</sup>X. Radu, A. Lapeyronne, and C. Craeye, "Numerical and experimental analysis of a wire medium collimator for magnetic resonance imaging," *Electromagnetics* **28**, 531–543 (2008).
- <sup>12</sup>X. Radu, D. Garray, and C. Craeye, "Toward a wire medium endoscope for MRI imaging," *Metamaterials* **3**, 90–99 (2009).
- <sup>13</sup>E. Shamonina, V. A. Kalinin, K. H. Ringhofer, and L. Solymar, "Magneto-inductive waveguide," *Electron. Lett.* **38**, 371–373 (2002).
- <sup>14</sup>L. Solymar, O. Zhuromskyy, O. Sydoruk, E. Shamonina, I. R. Young, and R. R. A. Syms, "Rotational resonance of magnetoinductive waves: Basic concept and application to nuclear magnetic resonance," *J. Appl. Phys.* **99**, 123908 (2006).
- <sup>15</sup>C. E. Hayes, W. A. Edelstein, J. F. Schenck, O. M. Mueller, and M. J. Eash, "An efficient, highly homogeneous radiofrequency coil for whole-body NMR imaging at 1.5 T," *J. Magn. Reson.* **63**, 622–628 (1985).
- <sup>16</sup>J. Tropp, "The theory of the bird cage resonator," *J. Magn. Reson.* **82**, 51–62 (1989).
- <sup>17</sup>R. R. A. Syms, T. Floume, I. R. Young, L. Solymar, and M. Rea, "Flexible magnetoinductive ring MRI detector: Design for invariant nearest neighbour coupling," *Metamaterials* **4**, 1–14 (2010).
- <sup>18</sup>R. R. A. Syms and L. Solymar, "Noise in metamaterials," *J. Appl. Phys.* **109**, 124909 (2011).
- <sup>19</sup>R. R. A. Syms, O. Sydoruk, and L. Solymar, "Lossy metamaterials: No effective medium properties without noise," *Phys. Rev. B* **84**, 235150 (2011).
- <sup>20</sup>G. C. Hurst and G. J. Mistic, "Coils for insertion into the human body," in *Encyclopedia of Nuclear Magnetic Resonance*, edited by D. M. Grant and R. K. Harris (John Wiley & Sons, Chichester, 1996), pp. 1373–1378.
- <sup>21</sup>S. Weiss, P. Vernickel, T. Schaeffter, V. Schulz, and B. Gleich, "Transmission line for improved RF safety of interventional devices," *Magn. Reson. Med.* **54**, 182–189 (2005).
- <sup>22</sup>A. Krafft, S. Müller, R. Umathum, W. Semmler, and M. Bock, "B<sub>1</sub> field-insensitive transformers for RF-safe transmission lines," *Magn. Reson. Mater. Phys.* **19**, 257–266 (2006).
- <sup>23</sup>R. R. A. Syms, L. Solymar, I. R. Young, and T. Floume, "Thin-film magneto-inductive cables," *J. Phys. D: Appl. Phys.* **43**, 055102 (2010).
- <sup>24</sup>R. R. A. Syms, I. R. Young, M. M. Ahmad, S. D. Taylor-Robinson, and M. Rea, "Magneto-inductive catheter receiver for magnetic resonance imaging," *IEEE Trans. Biomed. Eng.* (submitted).